ACS OMEGA

http://pubs.acs.org/journal/acsodf

Article

Electrical Properties of Thin $ZrSe_3$ Films for Device Applications

Lars Thole,* Christopher Belke, Sonja Locmelis, Peter Behrens, and Rolf J. Haug

Cite This: *ACS Omega* 2022, 7, 39913−39916

Read Online

ACCESS | Metrics & More | Article Recommendations | Supporting Information

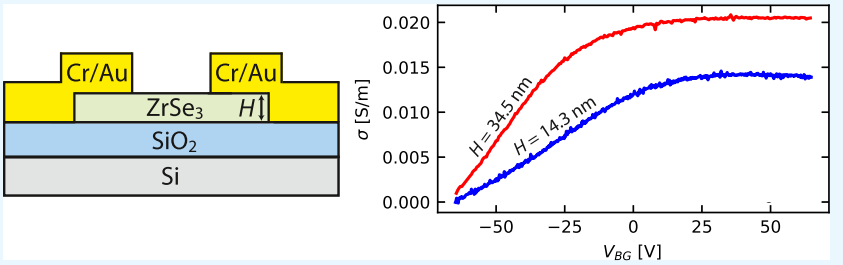

ABSTRACT: Measurements of key properties of the two-dimensional transition metal trichalcogenide $ZrSe_3$ are reported. The bulk material was created by chemical vapor deposition and subsequently exfoliated to obtain thin films of varying thicknesses. The samples were then characterized by atomic force microscopy measurements and Raman spectroscopy and contacted by e-beam lithography. Electrical measurements give values for the band gap energy of 0.6 eV increasing for thinner samples. Transistor measurements show $ZrSe_3$ to be an n-type semiconductor. By looking at several samples with varying thicknesses, it was possible to determine a mean free path of 103 nm for the bulk material which opens the possibility for new electronic devices.

INTRODUCTION

The field of two-dimensional (2D) materials offers a lot of new and interesting properties which has led to an increase in research in this area. There are plenty of 2D materials that show a wide variety of properties, creating new possibilities for applications, with the most famous example being graphene.[1−3] Because graphene lacks a band gap, a goal in recent research is the search of 2D semiconductors with different band gaps for different applications. In the field of semiconductors, the family of transition metal chalcogenides offers a wide range of materials. The best known group is the transition metal dichalcogenides (TMDCs) such as MoS_2.[4−6] Similar to the well-known group of the TMDCs, the lesser researched group of transition metal trichalcogenides (TMTCs) features a large amount of materials with a broad variety of band gaps.[7−11] In contrast to the TMDCs, they show anisotropy and quasi-1d channels, showing the possibility for new electrical and optical properties.[12,13] Thin films have only been realized for a few TMTCs, such as TiS_3.[14,15] In this work, the TMTC zirconium triselenide ($ZrSe_3$) was exfoliated and subsequently thin films with a thickness down to 9 nm were investigated with a focus on electrical measurements.

RESULTS AND DISCUSSION

The exfoliation was performed using the standard mechanical Scotch-tape-method,[1,16] in which the obtained flakes were placed on a Si wafer with a 330 nm thick SiO_2 substrate layer. The highly doped Si functions as a backgate. Single flakes were searched with an optical microscope and their geometry was determined with atomic force microscopy (AFM). Figure 1a

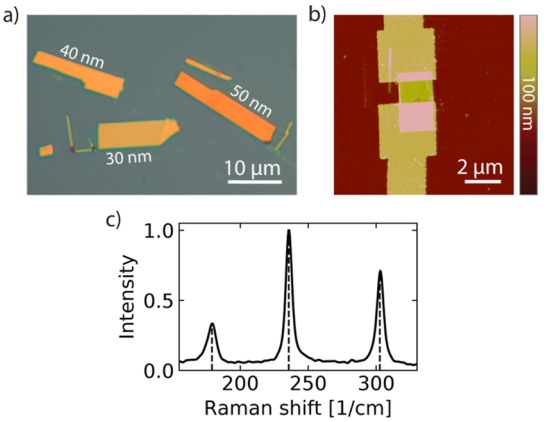

Figure 1. (a) Three flakes with less than 50 nm thickness. The value next to the flakes gives the average thickness of their homogeneous parts. It is possible to make estimates about the thickness from the color and the contrast on an optical picture. (b) AFM picture of a contacted flake with an average thickness of 34.5 nm. (c) Raman measurement of a flake with about 40 nm thickness.

Received: July 4, 2022
Accepted: September 22, 2022
Published: October 25, 2022

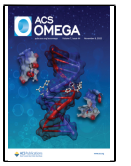

shows three flakes of different thicknesses under the optical microscope. The change in color with a varying thickness is typical for 2D materials and depends on the thickness of the used substrate.[17] Figure 1b shows a contacted sample with an average thickness of 34.5 nm as an AFM image. For further characterization, Raman spectroscopy was used. Figure 1c illustrates the Raman peaks for a flake with a thickness of about 40 nm. The positions of the peaks are at 179, 236, and 303 cm^{-1}, which is in good agreement with previous Raman measurements for the bulk material $ZrSe_3$.[18,19]

To conduct electrical measurements, standard e-beam lithography was used to create Cr/Au contacts on several flakes, one of which can be seen in Figure 1b, with different thicknesses ranging from 9 to 38 nm.

Figure 2 shows the changing of the current with temperature for a flake in an Arrhenius-plot. The current was determined

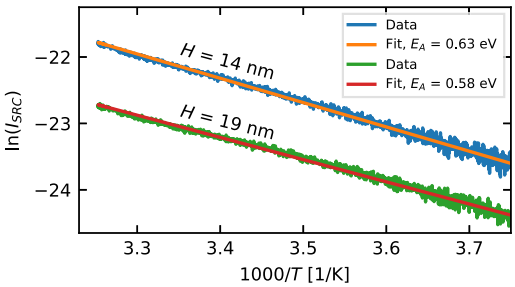

Figure 2. Arrhenius plot for two samples with different thicknesses H. Linear fits are shown in orange and red, respectively. For the sample with a thickness of 14 nm, an activation energy of 0.63 eV and for the sample with a thickness of 19 nm, an activation energy of 0.58 eV can be extracted.

from two-terminal measurements with a bias voltage of 1 V and a backgate voltage of 0 V. For a sufficiently high temperature, the current I of a semiconductor is proportional to $\exp(E_G/2k_B \cdot 1/T)$, where E_G is the band gap, k_B is the Boltzmann constant, and T is the temperature. By using a fit through our data (data shown in blue and green and fits in orange and red in Figure 2) it is possible to determine the band gap energy. The data shown in Figure 2 correspond to two samples with thicknesses of 14 and 19 nm and result in band gap energies of 0.63 and 0.58 eV, respectively, indicating a trend toward higher band gap energies for thinner samples. This trend is also seen in the few existing calculations where values of 0.68 and 0.75 eV have been determined for the bulk material which change to 0.92 and 1.17 eV for the monolayer, respectively.[8,12] Our determined values are slightly smaller but they clearly show the trend of smaller values for thinner samples.

The design of our samples allowed us to investigate transistor behavior. The 330 nm thick layer of SiO_2 on top of Si is used as a substrate for the dielectric layer in the field-effect transistor. Figure 3 shows the conductivity as a function of the backgate voltage for two flakes with significantly different thicknesses. The red curve shows the measured conductivity of a flake with a thickness of 34.5 nm and the blue curve of a flake with a thickness of 14.3 nm. A voltage of 0.4 V was applied to each of the samples while the backgate voltage was swept from −70 to +70 V. With the increase in gate voltage, the conductivity increases, until it reaches a saturation. The measurements show that nanosized $ZrSe_3$ is an n-type semiconductor as was previously also found for bulk $ZrSe_3$.[20]

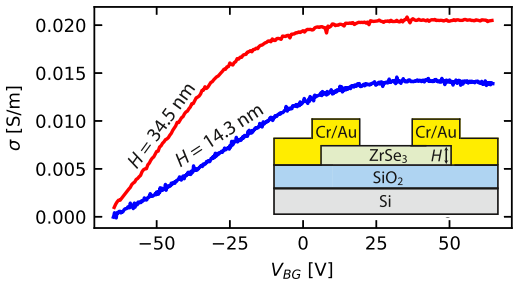

Figure 3. Conductivity (σ) of two flakes as a function of the backgate voltage (V_{BG}). The red curve is for a flake with 34.5 nm thickness and the blue curve for one with 14.3 nm thickness. Inset: schematic depiction of the sample.

We attribute this n-doping to the influence of the known Se vacancies. The saturation observed in Figure 3 can be attributed to the charge carrier density becoming constant. Changing the sweep direction showed a hysteresis effect, similar to the one previously reported for TiS_3[15,21] and MoS_2.[22,23] Figure 3 shows measurements sweeping the backgate voltage from negative to positive values. The linear parts of the curves give mobility values of 1.3×10^{-3} and 0.28×10^{-3} cm^2/V s for the 34.5 and 14.3 nm samples, respectively.

As it was already possible to see a change in the mobility for flakes with different thicknesses, we compared the resistivities for all our samples and found a thickness dependency as shown in Figure 4 using the classical size effect. The individual $V-I$

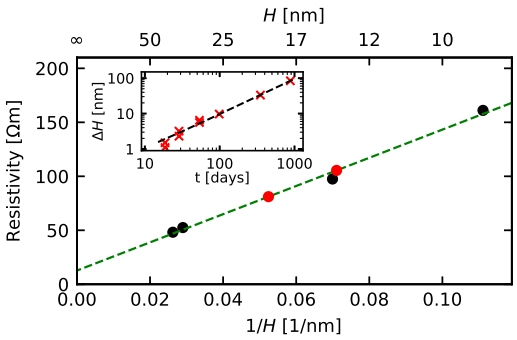

Figure 4. Resistivity as a function of the thickness H for different samples on the same wafer. The fit (dashed green line) gives values used for determining a mean free path of 103 nm for the bulk material. The red dots show values for measurements after the corresponding sample was exposed to air. Inset: layer growth on a flake with a starting thickness of 47.8 nm over several weeks.

measurements can be found in the Supporting Information. A fit through the measured data can be compared to the Drude model

$$\rho = \frac{m^* v_F}{ne^2}\left(\frac{1}{l_b} + \frac{1}{l_d}\right) \quad (1)$$

where ρ is the resistivity, m^* is the effective mass, v_F is the Fermi-velocity, n is the charge carrier density, e is the elementary charge, and l is the mean free path which is split into l_b and l_d according to the rule of Matthies. Here, l_d is the mean free path for scattering at the surfaces and l_b is the mean free path for scattering in the bulk. Because the width is significantly larger than the thickness H, we can assume that the thickness is the main limiting size. This means eq 1

https://doi.org/10.1021/acsomega.2c04198
ACS Omega 2022, 7, 39913−39916

becomes $\rho = \frac{m^* v_F}{ne^2}\left(\frac{1}{l_b}\right)$ for $1/l_d \rightarrow 0$, which is what happens when the samples become big enough so that scattering on the edge becomes almost irrelevant. Through the fit in Figure 4, we can extract a value ρ_0 of 12.7 Ω m for $1/H = 0$ and a value for $m^* v_F/ne^2$ of 1305.5 × 10^{-9} Ω m^2, given by the slope of the fit. Assuming that l_d is approximately the same as the thickness, we can extract a bulk mean free path l_b as 103 nm. Such a mean free path at room temperature is a rather large value, for example, in comparison to Si or elemental metals.[24,25]

For application purposes, the stability of a 2D material can be an important factor, for example, the 2D material $HfSe_2$ degrades quickly when left in air.[26] To test flakes of $ZrSe_3$ for stability, a flake with a starting thickness of 47.8 nm was measured with the AFM and then left on air at room temperature. This way, it was possible to see a homogeneous growth of the flake over a time period of about 800 days, as shown in the inset of Figure 4. Interestingly, the increase of thickness follows a linear behavior with a growth rate of about 0.1 nm per day. The linear behavior can be understood similar to the oxidation of silicon where this is also seen for shorter time spans.[27] Using the fit in Figure 4, it was possible to calculate an effective thickness, subtracting the isolating layer of oxide that grew on top of the four samples. Measuring the samples again after storing showed a degradation, leaving the two thinner samples non conductive and the two thicker samples with a reduced conductivity. With this method, we can see that the new effective thicknesses of the samples are about 20 nm smaller, explaining why the thinner samples are not conductive anymore as they would have completely degraded. For several TMDCs, a degradation process when left in air is known, and the nature of this process has been investigated to some extent.[26,28,29] In contrast to the TMDCs, the degradation of $ZrSe_3$ occurs very slowly, allowing for sample processing outside of a glovebox.

CONCLUSIONS

The material $ZrSe_3$ was synthesized by chemical transport and contacted by e-beam lithography. Thin films of $ZrSe_3$ were then investigated in reference to their thickness and electrical properties. We used an Arrhenius plot to find that the material shows a change in band gap energy with thickness from 0.63 eV for a thinner sample to 0.58 eV to a thicker sample. Furthermore, it was possible to see the transistor behavior in samples by applying a backgate voltage, showing that the material is an n-type semiconductor. Using samples with different thicknesses, a mean free path of 103 nm for the bulk material was found. Thin samples of $ZrSe_3$ show a very slow degradation behavior when exposed to air which opens the path to produce devices under ambient conditions.

METHODS

Sample Preparation. The bulk material $ZrSe_3$ was created by using a chemical transport method. The investigated compound was synthesized from the powdered elements in the molar ratio Se/Zr = 3 and with an excess of selenium (5% mass) to avoid the formation of the impurity phase ($ZrSe_2$). Purities of Zr and Se were 99.6 and 99.99%, respectively. Single crystals were grown in sealed evacuated quartz ampoules (length 150 mm, diameter 10 mm) in the presence of 5 mg of iodine per cm^3. Before the final chemical transport, giving rise to growth of single crystals, several sublimations forward and backward were accomplished in the quartz ampoule in order to improve the homogeneity of the batch which was then sintered at 650 °C for 7 days. The growth temperature was chosen as low as possible in order to preserve the stoichiometry. The sample was kept at a temperature gradient from T_2 (650 °C) to T_1 (600 °C) for 21 days. Scanning electron microscopy energy-dispersive X-ray analysis (JEOL, JSM-6610-NX) carried out on the well-crystallized products shows their purity and homogeneity as well as indicating an average composition of $ZrSe_{2.96}$. X-ray diffraction (XRD) data were collected at room temperature on a STADI P Stoe powder diffractometer, with Cu $K_{\alpha 1}$ radiation in the range $5 < 2\theta < 80$. The XRD confirms that the samples adopt the $P2_1/m$-structure. The lattice parameters a = 541.40(19) pm, b = 347.97(16) pm, c = 947.42(169) pm, and β = 97.442(55)° are in good agreement with previously reported structural data.[30−32] For XRD data, see the Supporting Information.

Measurement Methods. To conduct electrical measurements, a standard e-beam lithography process was used to create Cr/Au contacts on several flakes. The four samples used for electrical measurements were all on the same wafer, meaning they all went through the same processing steps. All of the electrical measurements were done as two-terminal DC measurements with a Keithley 2400 multimeter.

ASSOCIATED CONTENT

Supporting Information

The Supporting Information is available free of charge at https://pubs.acs.org/doi/10.1021/acsomega.2c04198.

XRD data for bulk $ZrSe_3$ and $V-I$ measurements of each sample (PDF)

AUTHOR INFORMATION

Corresponding Author

Lars Thole − *Institut für Festkörperphysik, Leibniz Universität Hannover, 30167 Hannover, Germany;* orcid.org/0000-0002-6468-6289; Email: thole@nano.uni-hannover.de

Authors

Christopher Belke − *Institut für Festkörperphysik, Leibniz Universität Hannover, 30167 Hannover, Germany*

Sonja Locmelis − *Institut für Anorganische Chemie, Leibniz Universität Hannover, 30167 Hannover, Germany*

Peter Behrens − *Institut für Anorganische Chemie and Laboratorium für Nano- und Quantenengineering, Leibniz Universität Hannover, 30167 Hannover, Germany*

Rolf J. Haug − *Institut für Festkörperphysik and Laboratorium für Nano- und Quantenengineering, Leibniz Universität Hannover, 30167 Hannover, Germany*

Complete contact information is available at: https://pubs.acs.org/10.1021/acsomega.2c04198

Notes

The authors declare no competing financial interest.

ACKNOWLEDGMENTS

This work was funded by the Deutsche Forschungsgemeinschaft (DFG, German Research Foundation) under Germany's Excellence Strategy—EXC 2123 Quantum Frontiers—390837967 and EXC 2122 PhoenixD—390833453 and within the Priority Program SPP 2244 "2DMP". The authors thank Marcel Schulz for providing help with the Raman measure-

ments and Adrian Hannebauer for help with further measurements.

REFERENCES

(1) Novoselov, K. S.; Geim, A. K.; Morozov, S. V.; Jiang, D.; Zhang, Y.; Dubonos, S. V.; Grigorieva, I. V.; Firsov, A. A. Electric field in atomically thin carbon films. *Science* **2004**, *306*, 666−669.
(2) Geim, A. K.; Grigorieva, I. V. Van der Waals heterostructures. *Nature* **2013**, *499*, 419−425.
(3) Novoselov, K. S.; Mishchenko, A.; Carvalho, A.; Castro Neto, A. H. 2D materials and van der Waals heterostructures. *Science* **2016**, *353*, aac9439.
(4) Mak, K. F.; Lee, C.; Hone, J.; Shan, J.; Heinz, T. F. Atomically thin MoS_2: A new direct-gap semiconductor. *Phys. Rev. Lett.* **2010**, *105*, 136805.
(5) Radisavljevic, B.; Radenovic, A.; Brivio, J.; Giacometti, V.; Kis, A. Single-layer MoS_2 transistors. *Nat. Nanotechnol.* **2011**, *6*, 147−150.
(6) Wang, Q. H.; Kalantar-Zadeh, K.; Kis, A.; Coleman, J. N.; Strano, M. S. Electronics and optoelectronics of two-dimensional transition metal dichalcogenides. *Nat. Nanotechnol.* **2012**, *7*, 699−712.
(7) Dai, J.; Li, M.; Zeng, X. C. Group IVB transition metal trichalcogenides: a new class of 2D layered materials beyond graphene. *Wiley Interdiscip. Rev.: Comput. Mol. Sci.* **2016**, *6*, 211−222.
(8) Li, M.; Dai, J.; Zeng, X. C. Tuning the electronic properties of transition-metal trichalcogenides via tensile strain. *Nanoscale* **2015**, *7*, 15385−15391.
(9) Abdulsalam, M.; Joubert, D. P. Structural and electronic properties of MX_3 (M = Ti, Zr and Hf; X = S, Se, Te) from first principles calculations. *Eur. Phys. J. B* **2015**, *88*, 177.
(10) Abdulsalam, M.; Joubert, D. P. Electronic and optical properties of MX_3 (M = Ti, Zr and Hf; X = S, Se) structures: A first principles insight. *Phys. Status Solidi B* **2016**, *253*, 868−874.
(11) Zhao, Q.; Guo, Y.; Zhou, Y.; Yao, Z.; Ren, Z.; Bai, J.; Xu, X. Band alignments and heterostructures of monolayer transition metal trichalcogenides MX_3 (M = Zr, Hf; X = S, Se) and dichalcogenides MX_2 (M = Tc, Re; X=S, Se) for solar applications. *Nanoscale* **2018**, *10*, 3547−3555.
(12) Jin, Y.; Li, X.; Yang, J. Single layer of MX_3 (M = Ti, Zr; X = S, Se, Te): A new platform for nano-electronics and optics. *Phys. Chem. Chem. Phys.* **2015**, *17*, 18665−18669.
(13) Island, J. O.; Molina-Mendoza, A. J.; Barawi, M.; Biele, R.; Flores, E.; Clamagirand, J. M.; Ares, J. R.; Sánchez, C.; van der Zant, H. S.; D'Agosta, R.; Ferrer, I. J.; Castellanos-Gomez, A. Electronics and optoelectronics of quasi-1D layered transition metal trichalcogenides. *2D Mater.* **2017**, *4*, 022003.
(14) Island, J. O.; Barawi, M.; Biele, R.; Almazán, A.; Clamagirand, J. M.; Ares, J. R.; Sánchez, C.; van der Zant, H. S.; Álvarez, J. V.; D'Agosta, R.; Ferrer, I. J.; Castellanos-Gomez, A. TiS_3 transistors with tailored morphology and electrical properties. *Adv. Mater.* **2015**, *27*, 2595−2601.
(15) Lipatov, A.; Wilson, P. M.; Shekhirev, M.; Teeter, J. D.; Netusil, R.; Sinitskii, A. Few-layered titanium trisulfide (TiS_3) field-effect transistors. *Nanoscale* **2015**, *7*, 12291−12296.
(16) Novoselov, K. S.; Jiang, D.; Schedin, F.; Booth, T. J.; Khotkevich, V. V.; Morozov, S. V.; Geim, A. K. Two-dimensional atomic crystals. *Proc. Natl. Acad. Sci. U.S.A.* **2005**, *102*, 10451−10453.
(17) Blake, P.; Hill, E. W.; Castro Neto, A. H.; Novoselov, K. S.; Jiang, D.; Yang, R.; Booth, T. J.; Geim, A. K. Making graphene visible. *Appl. Phys. Lett.* **2007**, *91*, 063124.
(18) Kurita, S.; Okada, Y.; Tanaka, M. Resonant Raman scattering in ZrS_3 and $ZrSe_3$. *Helv. Phys. Acta* **1985**, *58*, 321−328.
(19) Wieting, T. J.; Grisel, A.; Levy, F. Raman Scattering by Optical Phonons In $TaSe_3$ and $NbSe_3$. *Mol. Cryst. Liq. Cryst.* **1982**, *81*, 117−124.
(20) Patel, K.; Prajapati, J.; Vaidya, R.; Patel, S. G. Optical and electrical properties of $ZrSe_3$ single crystals grown by chemical vapour transport technique. *Bull. Mater. Sci.* **2005**, *28*, 405−410.
(21) Randle, M.; Lipatov, A.; Kumar, A.; Kwan, C. P.; Nathawat, J.; Barut, B.; Yin, S.; He, K.; Arabchigavkani, N.; Dixit, R.; Komesu, T.; Avila, J.; Asensio, M. C.; Dowben, P. A.; Sinitskii, A.; Singisetti, U.; Bird, J. P. Gate-Controlled Metal-Insulator Transition in TiS_3 Nanowire Field-Effect Transistors. *ACS Nano* **2019**, *13*, 803−811.
(22) Late, D. J.; Liu, B.; Matte, H. S.; Dravid, V. P.; Rao, C. N. Hysteresis in single-layer MoS_2 field effect transistors. *ACS Nano* **2012**, *6*, 5635−5641.
(23) Shah, P. B.; Amani, M.; Chin, M. L.; O'Regan, T. P.; Crowne, F. J.; Dubey, M. Analysis of temperature dependent hysteresis in MoS_2 field effect transistors for high frequency applications. *Solid-State Electron.* **2014**, *91*, 87−90.
(24) Qiu, B.; Tian, Z.; Vallabhaneni, A.; Liao, B.; Mendoza, J. M.; Restrepo, O. D.; Ruan, X.; Chen, G. First-principles simulation of electron mean-free-path spectra and thermoelectric properties in silicon. *Europhys. Lett.* **2015**, *109*, 57006.
(25) Gall, D. Electron mean free path in elemental metals. *J. Appl. Phys.* **2016**, *119*, 085101.
(26) Mirabelli, G.; McGeough, C.; Schmidt, M.; McCarthy, E. K.; Monaghan, S.; Povey, I. M.; McCarthy, M.; Gity, F.; Nagle, R.; Hughes, G.; Cafolla, A.; Hurley, P. K.; Duffy, R. Air sensitivity of MoS_2, $MoSe_2$, $MoTe_2$, HfS_2, and $HfSe_2$. *J. Appl. Phys.* **2016**, *120*, 125102.
(27) Deal, B. E.; Grove, A. S. General relationship for the thermal oxidation of silicon. *J. Appl. Phys.* **1965**, *36*, 3770−3778.
(28) Gao, J.; Li, B.; Tan, J.; Chow, P.; Lu, T.-M.; Koratkar, N. Aging of Transition Metal Dichalcogenide Monolayers. *ACS Nano* **2016**, *10*, 2628−2635.
(29) Qiu, H.; Pan, L.; Yao, Z.; Li, J.; Shi, Y.; Wang, X. Electrical characterization of back-gated bi-layer MoS_2 field-effect transistors and the effect of ambient on their performances. *Appl. Phys. Lett.* **2012**, *100*, 123104.
(30) Krönert, W.; Plieth, K. Die Struktur des Zirkontriselenids $ZrSe_3$. *Z. Anorg. Allg. Chem.* **1965**, *336*, 207−218.
(31) Brattås, L.; Kjekshus, A.; Krogh-Moe, J.; Songstad, J.; Pilotti, Å. On the Properties of Compounds with the $ZrSe_3$ Type Structure. *Acta Chem. Scand.* **1972**, *26*, 3441−3449.
(32) Furuseth, S.; Brattås, L.; Kjekshus, A.; Andresen, A. F.; Fischer, P. On the Crystal Structures of TiS_3, ZrS_3, $ZrSe_3$, $ZrTe_3$, HfS_3, and $HfSe_3$. *Acta Chem. Scand.* **1975**, *29a*, 623−631.

https://doi.org/10.1021/acsomega.2c04198
ACS Omega 2022, 7, 39913−39916